Validation of the CFD method for determining the measurement error in Flare Gas Ultrasonic meter installations

Jeff Gibson, TUV NEL

1 INTRODUCTION

This paper discusses the results of an ongoing project assessing the effectiveness of using Computational Fluid Dynamics (CFD) modelling to predict the installation error on a single-path flare gas ultrasonic flowmeter. The work is being funded through the National Measurement Office's (NMO) Engineering and Flow Programme (www.flowprogramme.co.uk) and will be detailed in TUV NEL report 2008/301 [1]. The CFD simulations were compared with experiments undertaken in TUV NEL's National Standard Atmospheric Flow Measurement Facility.

Tests were performed using a 1.5D-radius single bend placed at various pipe diameters (D) from the inlet flange of the meter. The experimental work was conducted using ultrasonic transducers supplied by GE Sensing. The transducers were installed in a specially-made 12-inch meter spool to allow the error to be assessed at the commonly used diametric and mid-radius positions. The meter was tested from 0.25 m/s to 30 m/s corresponding to a range of Reynolds numbers of 5,000 to 600,000, the Reynolds numbers at the lower end being such that the flow was likely to be in laminar-turbulent transition. Such flows are not uncommon in emergency flare systems during routine day-to-day flaring. The flow simulations were undertaken using the commercial CFD package Fluent™.

The work described in this paper demonstrates the capabilities of the TUV NEL low-pressure test facility for determining the installation error in flare gas ultrasonic meters. In addition, CFD modelling has proved to be a very useful tool for determining the installation errors, also helping to interpret and rationalise the experimental data.

A follow-up project is underway to further investigate the issues raised by the initial phase of work and this will be briefly discussed in this paper.

2 BACKGROUND

Flaring from UK oil and gas facilities is controlled and regulated through the Flare Consent Scheme operated by the Department of Energy and Climate Change (DECC). Operators are also required to report their calculated CO_2 emissions resulting from gas flaring, and fuel usage, into the EU Emissions Trading Scheme (EU ETS).

Fig. 1 – Gas flaring from an offshore oil and gas platform

With CO_2 credits being a tradable commodity within the EU ETS, the operator has an incentive to reduce the amount of gas flared below their permitted level. However, the importance of obtaining accuracy on the determination of the quantity of gas flared, and therefore the mass of CO_2 released to atmosphere, is very clear. To this end the EU ETS prescribes uncertainty levels which must be achieved in order to comply with the regulations (Directive 2003/87/EC [2]). The requirements for measurement and reporting flare are given within Annex II, Section 2.1.1.3 of the accompanying Measurement and Reporting Guidelines 2007 (MRG 2007 [3]).

Installations covered by the EU ETS are categorised depending on total CO_2 emissions. For the oil and gas sector this is mostly made up of the CO_2 emitted from the burning of produced gas as a fuel, with the remainder being made up of flaring and the burning of liquid fuels such as Diesel oil etc. The higher the category (i.e. "Tier Level"), the lower the required uncertainty. Section 5.2 of Annex I of the MRG states that:

"The highest tier approach shall be used by all operators to determine all variables for all source streams for all Category B or C installations. Only if it is shown to the satisfaction of the competent authority that the highest tier approach is technically unfeasible, or will lead to unreasonably high costs, may a next tier be used for that variable within a monitoring methodology".

The maximum allowable activity data (volume or mass) uncertainty for flaring under category A, B and C installations is stated 17.5%, 12.5% and 7.5% (corresponding to tiers 1, 2 and 3 respectively). The majority of UK offshore installations fall into Category B. UK operators must therefore be able to demonstrate to the regulator that they are meeting 12.5% and the uncertainty calculations must also be verified by an accredited third-party. There are some larger, Category C platforms in the Norwegian and Danish sectors of the North Sea.

Ultrasonic meter manufacturers state the uncertainty on their flare meters based on ideal, fully developed flow conditions where there are no entrained liquids in the gas and the critical dimensions are accurately measured. Therefore, it is important to consider the effect of any deviations from the ideal in subsequent uncertainty analyses of flare meters as installed and used in the field.

An important aspect that must be considered in the uncertainty analysis arises from the piping configuration upstream and downstream of the meter. Upstream fittings will disturb the flow and will result in an installation error. An approach to determining this error is discussed in this paper.

3 FLARE GAS ULTRASONIC METERING

Ultrasonic meters are the most developed and widely used technology for flare gas measurement, with thousands of meter installations worldwide. The main advantages are a wide rangeability in velocity, no moving parts and virtually zero pressure drop – a mandatory requirement in an emergency flare line. An additional advantage of ultrasonic transit-time meters is their ability to determine molecular weight, and hence density of the gas, from speed of sound measurement. Relevant standards for general ultrasonic gas flow meters include ISO TR 12765 [4] and BS 7965 [5]; BS 7965 provides some guidance on the application of ultrasonic meters to flare measurement under its Class 4 category of meters.

Depending on the meter type and line size, the velocity range of a flare gas ultrasonic meter is quoted as between 0.03 m/s to 100 m/s. Uncertainty for a flare gas ultrasonic meter is typically specified by the manufacturers as 2.5 - 5% on velocity across the range 0.3 – 80 m/s, increasing as velocity reduces. However, these specifications are only strictly applicable under ideal flowing conditions (i.e. relatively stable, fully developed flows that are free of liquid droplets, solids and ultrasonic noise generated by valves etc. with the critical dimensions accurately measured).

Any additional uncertainty arising from deviations from the ideal must be added to the quoted baseline uncertainty to arrive at the total uncertainty figure. These additional uncertainty components should be considered when determining the overall figure for emissions reporting purposes. Hydrocarbon Management Committee document HM58 [6], published by the Energy Institute, Aberdeen provides guidance on the determination of flare gas quantity for environmental reporting purposes. It includes a section identifying the sources of uncertainty on a flare gas ultrasonic meter and a methodology of determining and correcting for installation error.

3.1 Installation of Ultrasonic Flare Gas Meters

Operators have the opportunity to fit spool-pieced flare meters into new oil and gas facilities. However, older installations will not have had a flare meter installed during construction. Therefore, unless production can be stopped for a period to allow breaking into the line, meters will likely have to be retrofitted to the existing flare line using either cold- or hot-tap welding techniques.

Space on offshore oil and gas platforms is at a premium and, as a result, it is often impossible to meet the upstream and downstream length requirements specified by the meter manufacturers to ensure that there is no additional uncertainty in the measurement. These are most commonly stated as 20 straight pipe diameters (20D) upstream and 5 or 10D downstream.

One of the key issues regarding flare gas meter uncertainty is the effect of upstream installation on flow profile. Fixtures such as bends, valves and reducers tend to disturb the flow such that the velocity profile deviates from the ideal, axi-symmetric shape. An error occurs because the calculation of average velocity (and hence volumetric flow) relies on a correction factor that is based on the assumption of an ideal flow profile. In addition to a change in the shape of the axial flow profile, non-axial velocity components (causing the flow to swirl) will also affect the meter reading. It is also worth noting that increased turbulence generated by some fittings may also cause problems with repeatability, especially when the meter is in close proximity to the fitting.

Flare-gas ultrasonic meters generally employ a single, wetted beam-path which means that they are particularly sensitive to flow profile compared with multipath meters. Dual-path designs are also available which provide an improvement in uncertainty. The work summarised in this paper concentrates on the more common single-path design.

3.2 The GE Sensing GF868 Flare Gas Ultrasonic Meter

The GF868 ultrasonic flare gas meter comprises two ultrasonic transducers inserted into the flare gas line through bosses welded onto the pipework). The transducers can be installed in various path configurations to allow ease of access, but are often inserted from the top of the pipe (Fig. 2). The transducers may be installed through isolation valves allowing retraction of the transducers for maintenance and inspection purposes without the need to shut down the process.

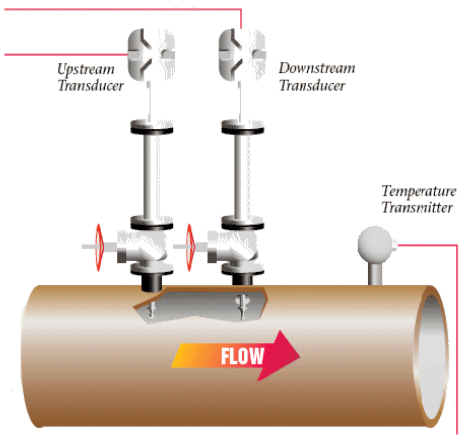

Fig. 2 - General Arrangement of the GF868 meter (www.gesening.com)

The flare gas meter measures velocity along the path, which usually at an angle of 45° to the flow. This is then converted to an average velocity via a correction factor; average volumetric flowrate can be calculated through input of the meter internal diameter. Volume flowrate can be calculated at standard reference conditions using a measurement of temperature and pressure. Finally, density and, therefore, mass flow can be calculated from speed of sound measurement, temperature (and in more recent designs, pressure) using a proprietary correlation for average molecular weight.

GE Sensing supplied a dual-channel GF868 flare gas ultrasonic meter to TUV NEL for testing in July 2008. This allowed for two separate, single path measurements to be read by switching between the channels in alternation. The purpose of the dual-path meter was to assess the effect of installation on two different path positions during an installation test. This is of interest as smaller meters (typically < 14-inch) will tend to have a diametric path, whilst larger meters will tend to have a mid-radius path.

3.2.1 Spool piece and meter configuration

A spool piece was manufactured by GE Sensing in order to house the ultrasonic transducers at the diametric and mid-radius positions within a 12" Sch. 20 pipe (i.d. 311 mm), as shown in Fig. 3. The transducers are inserted through four, 3-inch (76 mm) i.d. flanged bosses. With the flow direction from left-to-right in Fig. 3, the diametric path is upstream of the mid-radius path, three pipe diameters (3D) from the inlet flange of the meter spool. The mid-radius path is 3D downstream of the diametric path in the same plane, but offset in upper portion of the pipe by half the pipe radius (R/2 = 77.75 mm). Both paths were aligned at 45° to the flow. Pressure and temperature were measured at 2D and 3D downstream of the mid-radius channel respectively.

The meter was set up to take the average of 32 readings of transit time difference, Δt, from each channel, the electronics periodically alternating between channels. The sequence of obtaining the 32 readings, processing and averaging took approximately 7 seconds for each channel. The output from the two meter channels was read by TUV NEL's data acquisition system via two separate 4-20 mA signals.

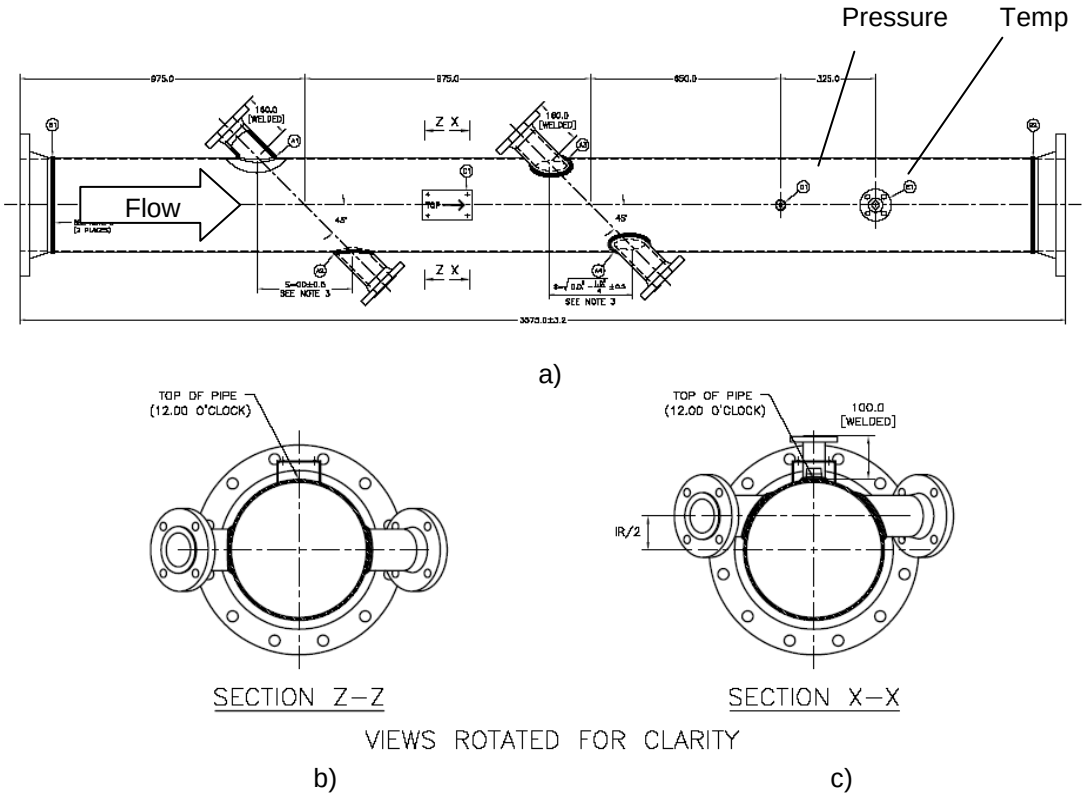

Fig. 3 - Dimensioned Drawing of the 12" Spool Housing the two Sets of Ultrasonic Transducers: a) Plan View of Spool, b) End View of Diametric Path, c) End View of Mid-Radius Path

Figure 4 shows a close-up detail of the transducers installed in the bosses for the diametric (Fig. 4a) and mid-radius (Fig. 4b) path positions respectively. The transducers were set such that the path length was the same (329 mm) in both cases, meaning that the mid-radius transducers were retracted into the boss about 30 mm further back than the diametric path.

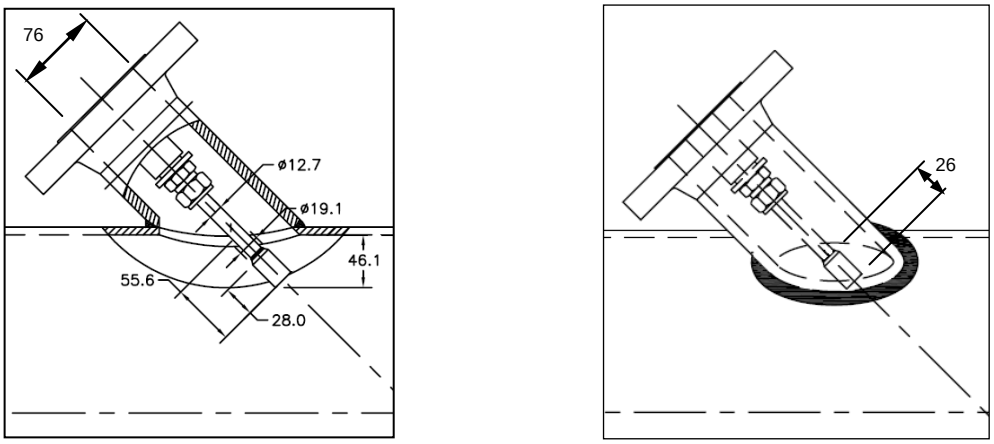

Fig. 4 - Detail of the Transducers at: a) Diametric, and b) Mid-radius Positions (Dims. in mm)

The meter determines the mean flow velocity along the length of the ultrasonic beam-path by measuring the difference in time taken for the ultrasonic pulses to pass between the transducer pair in the upstream (t_{21}) and downstream (t_{12}) directions in rapid succession. When gas is flowing, the beam will take longer to travel in the upstream direction (against the flow) compared with the downstream (with the flow); therefore $t_{21} > t_{12}$.

It can be shown that the path velocity, v_p, is a function of the meter geometry and the transit time difference, Δt, and is thus independent of the speed of sound

$$v_p = \frac{L}{2\cos\phi}\frac{\Delta t}{t_{21}t_{12}} \tag{1}$$

Assuming ideal flow conditions, with a fully developed velocity profile in the meter, the mean flow velocity across the pipe cross-section, $\bar{v}$, and hence the volumetric flowrate, *Q*, can be calculated thus:

$$\bar{v} = kv_p \tag{2}$$

and

$$Q = \bar{v}\pi R^2 \tag{3}$$

The meter factor, k, is used to convert measured path velocity to a mean pipe velocity and is normally set to a value based on the assumption of an ideal, fully developed flow profile. The meter factor is usually set as variable with Reynolds number for a diametric path and constant for a mid-radius path. Since the reference flow was measured during the TUV NEL tests, the meter factor was simply set as 1.0 for both the diametric and mid-radius channels. In doing so this allowed k to be determined by simply dividing the reference velocity through the meter (as calculated from the reference mass flowrate, local density and meter diameter), with the average velocity output by the meter (also based on the same diameter).

4 INSTALLATION EFFECT TESTS

Table 1 summarises the tests performed on the flare gas meter. The installation error was determined by comparing the velocity output obtained at the two path positions with the single bend at various locations upstream of the meter with that measured under baseline conditions. Curve fits were applied to the two baseline data sets to ensure that the comparison was undertaken at the same velocity.

The installation effect tests were performed with the bend in the vertical orientation relative to the meter. The bend was placed 5, 10, 20 and 45D from the meter inlet flange and the

installation error was determined at 0.25, 0.5, 4, 7, 15 and 30 m/s respectively. The equivalent pipe Reynolds numbers are as given in Table 1. The baseline test was repeated at the lower velocity end following unexpected results at such low Reynolds numbers.

Table 1 – Summary of tests carried out on the meter

	Nominal Velocity (m/s)	Nominal Volume flow (m^3/hr)	Nominal Reynolds numbers
Baseline test	0.25 – 30	68 – 8,200	5,000 – 600,000
Bend at 5D	0.25 0.5 4 8 15 30	70 140 1,000 2,200 4,100 8,200	5,000 10,000 80,000 160,000 300,000 600,000
Bend at 10D	as above	as above	as above
Bend at 20D	as above	as above	as above
Bend at 45D	as above	as above	as above
Repeat baseline	0.25 – 1.5	70 – 400	5,000 – 30,000

Figure 5 shows a schematic of the Atmospheric Gas Flow Measurement Facility for the baseline and installation test cases. Ambient air under a slight vacuum was drawn into the test line from the gas flow laboratory via a 70 kW, centrifugal fan which vents into a basement area. The fan runs at a constant speed and the flowrate through the test section is set by adjusting a bypass section and/or a set of guide vanes. The fan can deliver up to around 15,000 m^3/hr depending on pressure drop. Figure 6 shows a photograph of the test meter as installed in the specially made spool-piece. Insulation material was fixed to the crown of the pipe following some issues with noise on the readings from the mid-radius channel. This approach is commonly used in the field to attempt to attenuate ultrasonic waves which may be "leaking" from one transmitter to the other across the surface of the pipe. Although there was variability in the signal-to-noise levels, the magnitude of the noise was not thought to be too serious and the testing was progressed regardless.

In the baseline case (Fig. 5a) there was 45D of straight pipe upstream of the meter inlet flange (giving 48D to the diametric and 51D to the mid-radius paths respectively). Figure 5b details the pipework configuration for the case with the bend at 45D from the meter inlet flange. In this case, the bend was simply attached to the end of the pipe that had previously served as the inlet for the baseline tests.

Reference flow rate was measured by one of four orifice plates (of diameter ratio, β = 0.2, 0.3, 0.5 and 0.75) installed in an 8-inch holder. There was 30D of straight length upstream of the orifice plate holder and 8D downstream of it. The orifice plates were calibrated over an equivalent Reynolds number range in TUV NEL's water-flow facility, which is the primary standard for the UK. The expansibility equation in ISO 5167:2 [7] was then used to correct for changes in throat density due to temperature changes.

The uncertainty in the reference mass flowrate for the test facility orifice plates is calculated to be 0.5% (95% confidence). However, given the comparative nature of installation effect testing, repeatability is more important than the uncertainty. The repeatability on the measurements was found to be dominated by the scatter on the average velocity obtained by the meter as will be discussed later.

Figure 7 shows a photograph of the bend inlet section at 10D from the meter inlet flange. The bend included a 10D inlet length to allow the flow to reattach to the pipe wall on entry before reaching the bend. Care was taken to ensure that the plane of the bend was aligned with the meter.

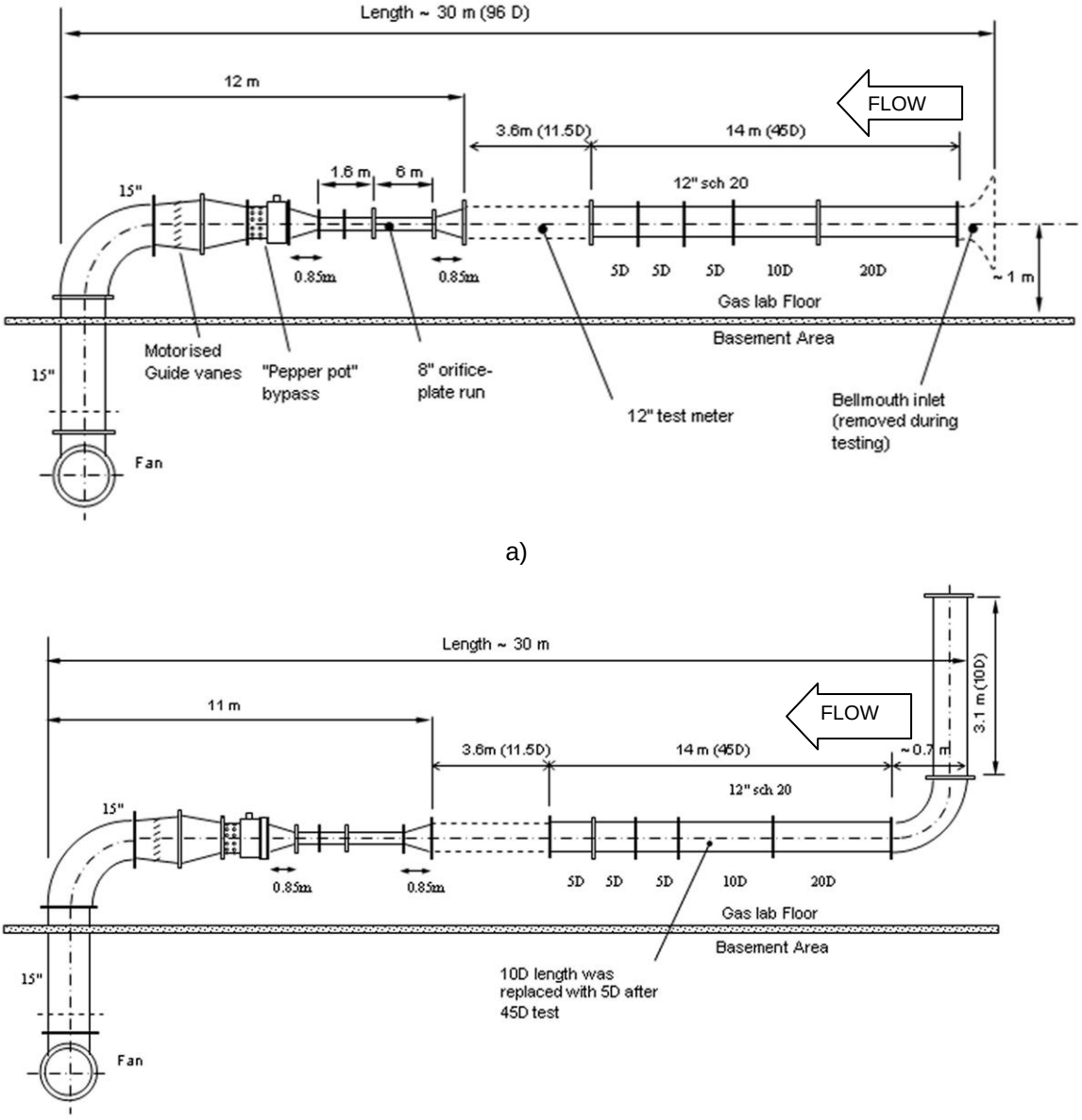

Fig. 5 – Schematics of the configuration used to test the flare gas meter: a) baseline tests, b) single bend tests (note: not to scale).

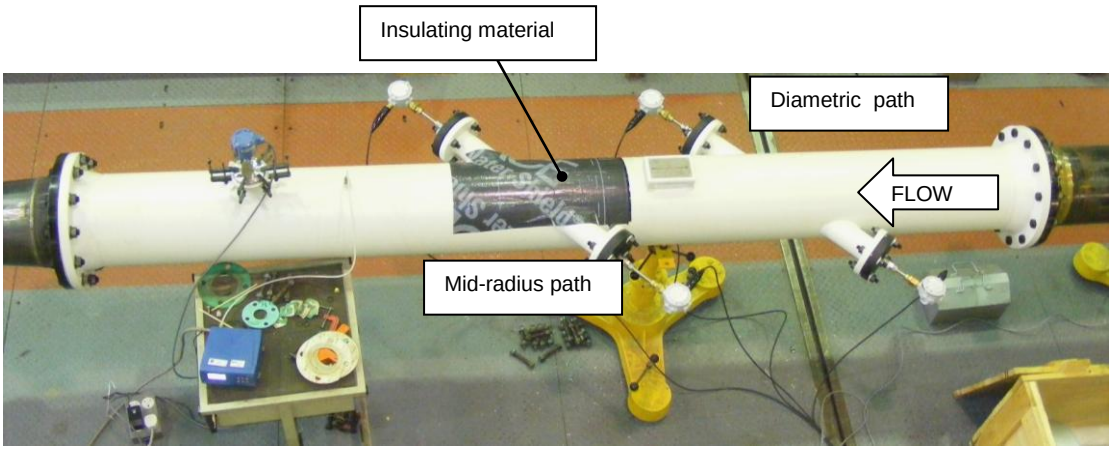

Fig. 6 - Detail of the Transducers and Bosses at: a) Diametric, and b) Mid-radius Positions

Fig. 7 – Single bend installation

4.1 Data Acquisition and Instrumentation Used

The resolution of the digital reading of transit time was 0.01 m/s. The output signal from the two ultrasonic meter channels was 4-20 mA and these were recorded by two separate channels in an Agilent data logger. The resolution on the measured current was 4.8 μA.

The full-scale value at 20 mA was adjusted as velocity decreased to ensure that the resolution error did not exceed 0.25% on velocity at the lowest measured current (6 mA). It was therefore most convenient to adjust the full scale during changeover of the reference orifice plate.

All instrumentation was calibrated using equipment traceable to National standards. Static pressure at the orifice plate and ultrasonic meter was measured using two Druck DPI 142 absolute pressure gauges. Temperature was measured at the orifice plate using a 4-wire PRT and at the ultrasonic meter using a 4-wire Emerson PT100 sensor mounted in a thermowell. All temperature measurements were logged via precision resistors within an Agilent data logger. The temperature probes were calibrated in a heated bath over the range 0 to 60°C to an uncertainty of better than 15 mK, which equates to 0.005% at 20°C.

Differential pressure across the reference orifice plate was measured using a Yokogawa DP Harp EJX110A digital sensor calibrated against a dead weight tester to better than 0.08% (95% confidence) over the range 100 - 20,000 Pa. The lowest differential pressure measured during the tests was about 500 Pa.

The absolute pressure sensors were calibrated to an uncertainty of better than 6 Pa (95% confidence) across the range 750 – 1150 mbar, equating to 0.06% (95% confidence) at atmospheric pressure.

Ambient pressure, temperature and humidity close to the inlet of the test line were recorded at the start of a test and assumed to be constant over its duration. The humidity was corrected to the pressure and temperature conditions at the ultrasonic meter and orifice plate respectively so that the air density could be calculated at these positions. The humidity sensor was calibrated to an uncertainty of better than ± 1% of relative humidity (e.g. at RH = 50%, the actual reading will be somewhere between 49% and 51%)

4.1.1 Stability issues

Given the comparative nature of installation effect testing, it is the repeatability of the results, rather than the overall uncertainty, that is most important. During testing it was noted that the standard deviation on the meter velocity was much higher than on the reference flow rate and tended to dominate the repeatability in the results. Repeatability became an issue below about 1 m/s. The main reasons for this were:

- The resolution on the digital output of velocity was limited to ± 0.01 m/s. This translated to ± 4% on an individual reading at the lowest velocity of 0.25 m/s, reducing to 1% at 1 m/s and 0.03% at 30 m/s. In theory at least, the uncertainty on the average velocity logged during the test point reduces with the square-root of the number of sample points. It should also be noted that GE Sensing quote an uncertainty on velocity of ± 20% over the range 0.03 to 0.3 m/s.
- The protruding diametric probes caused instability to the velocity on the mid-radius path, particularly at lower velocities where the flow was straddling the laminar-turbulent transition region.
- The logging speed was slowed down by the use of a single flow computer to switch between the two measurement channels in alternation. This, together with the molecular weight calculation (which could not be switched off), incurred a delay of about 7 seconds between readings thus limiting the number of readings which could be taken over a reasonable time period.
- Even at zero flow the signal-to-noise level on the mid-radius path, although of a high enough magnitude, was seen to be variable and this may have contributed to the stability of the reading.

The above issues are being addressed in the next phase of the project (as listed in the further work section of this paper).

5 CFD MODELLING OF THE FLARE GAS ULTRASONIC METER

The CFD modelling was undertaken using Fluent v6.2.3 solver and post-processing package and Gambit v2.4.6 meshing software [8]. The default parameters for air were used to model the flow:

Density 1.225 kg/m^3
Viscosity 1.784 ×10^{-5} kg/m-s

The flow was assumed to be steady and incompressible throughout. The realisable k-ε turbulence model was used in most cases. More information on the CFD method, and turbulence modelling, can be found in standard texts [9].

The CFD modelling of the ultrasonic meter was undertaken in three separate stages:

1. Bend model
2. Baseline model
3. Meter model

The bend and baseline models are run in order to generate the inlet boundary conditions for the meter model at each given flowrate. The velocity in the x, y and z directions, and turbulence parameters, at the relevant locations are then transferred from these two models to the relevant meter model via so-called “profile files”.

The grid geometry of the bend model is shown in Fig 8. The flow at the inlet was modelled using a cube-shaped pressure boundary. This allowed air to be drawn into the pipe from all directions and along the outer surface of the pipe. The grid employed a total of 2.5 million computational cells. The majority of these were triangular prisms which were concentrated inside the pipe. The cross sectional grid (inset of Fig. 8) was made up of triangular elements that exactly matched the grid of the meter model (Fig. 9) so as to minimise interpolation errors. The baseline model was similar to the bend model except that the bend was replaced with the 50D length of straight pipe. This model had a total of 1.7 million cells.

The pipe wall and inlet flange were set as smooth and a no-slip boundary condition (i.e. velocity is zero at the wall in all directions) was assumed. The standard wall function model was used to calculate the flow properties in the cell immediately adjacent to the pipe wall. The flange at the inlet of the 10D pipe was also included in the model.

Figure 9 shows the computational mesh on the walls of the flare gas ultrasonic meter with the wetted portion of the transducers included. The meter model used just under 2 million cells with the grid being concentrated around the transducers and along the beam paths (indicated by the dotted lines). The mesh is refined local to the transducers and was structured and uniform along the beam paths. To minimise interpolation errors - and to ensure a smooth, regular velocity curve was obtained from each path - the grid (and beam paths) were constructed such that the path passed directly through each of the 66 node points on the line. Several integration methods were used to determine an average velocity along the beam paths, but it was found that a step-wise, area weighted-average was adequate (this is a standard reporting option within Fluent).

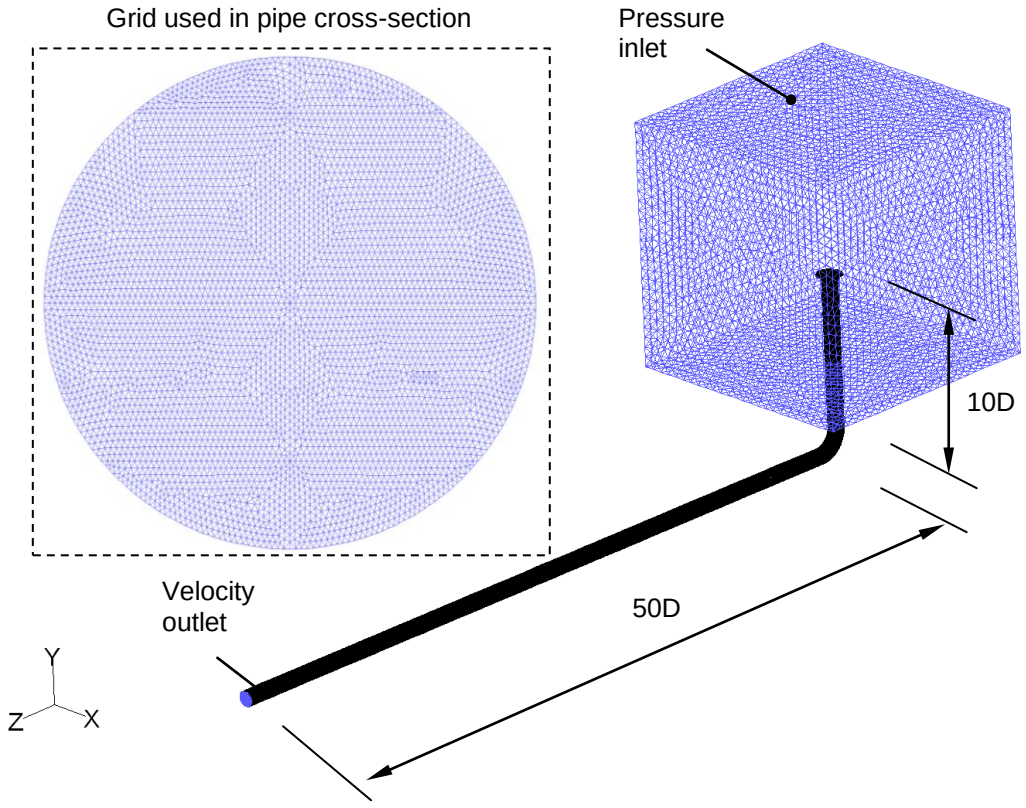

Fig. 8 – Mesh and geometry used to simulate the upstream bend installation

5.1 Method of Determining Installation Error Using CFD

Figure 9 details the computational grid used to model the flare gas meter with the beam paths superimposed onto it. The average velocity in the flow direction, v, is calculated from the average velocity in the direction of the path, v_p, using

$$v = \frac{v_p}{\cos\phi}, \tag{4}$$

where ϕ is the beam angle (45°).

The meter factor, *k*, is given by the ratio of the mean pipe velocity, $\bar{v}$, to the axial velocity by

$$k = \frac{\bar{v}}{v} \tag{5}$$

The meter error is then expressed as:

$$\%Error = \left(\frac{k_b - k_i}{k_i} \right) \times 100 \tag{6}$$

where k_i is the meter factor calculated for the relevant installation and k_b is the meter factor calculated for the baseline case.

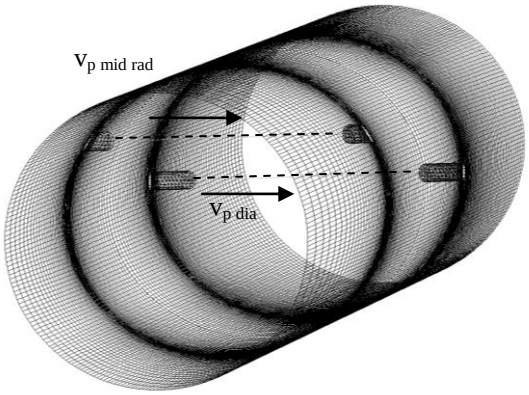

Fig. 9 – Grid on the wall of the flare meter model including transducer tips (dotted lines = beam paths).

6 COMPARISON OF CFD RESULTS WITH TEST DATA

Figure 10 compares the results of the installation error plotted against distance from the bend to the beam path for the diametric path at 0.25, 0.5, 4 and 30 m/s respectively. These equate to approximate pipe Reynolds numbers of Re_D = 5,000, 10,000, 80,000 and 600,000.

The CFD predicts the correct general trend for the diametric path starting off as negative and (but for one point on the 0.25 m/s curve) reducing in magnitude towards zero as distance from the bend increases. The CFD results are within 2 - 4% of the test data for velocities above 4 m/s and between 4 - 6%, for velocities below 0.5 m/s. The CFD model also correctly predicts the more rapid flattening-off of the error trend with distance from the bend which occurs at the lower velocities. However, it is noted that the test data generally lies below the CFD data (i.e. a higher negative error is evident) and is more velocity-dependent.

The CFD does not agree well with the test data for the mid-radius path, both in terms of the magnitude of the error and the general trend (Fig. 11). The error is of the opposite sign and the shapes of the curves are almost the mirror-image of the test data. The reason for this is the subject of ongoing research but it is thought to be largely due to non-ideality in the tests. It is anticipated that the mid-radius path is much more sensitive to swirl and flow profile than the diametric path and may have been adversely affected by the disturbance to the flow caused by the upstream diametric path.

Although some deviation would have been expected at the lowest velocity of 0.25 m/s, the resulting error trend was unexpected – the error actually increasing with distance from the bend.

A repeat of the baseline results revealed that there was an issue with reproducibility of the baseline results at 0.5 m/s and, especially, at 0.25 m/s, which is most likely due to laminar-turbulent transition occurring and, therefore, instability in the flow profile. There was also high scatter observed on the mid-radius data at this flowrate which was likely due to a combination

of the flow regime and the disturbance caused by the protruding transducers of the diametric path.

GE Sensing were consulted during the project and provided the following feedback:

- The mid-radius path is not normally used on flare lines of less than 14-inch diameter with the result that there would have been increased interaction between the transducer and the wall during the tests in 12-inch line
- The disturbance from the protrusion of the diametric transducers would likely have caused problems with the mid-radius path.
- The diametric transducers could have been retracted to the wall and did not need to be set such that the distance between them was the same as for the mid-radius path.
- GE Sensing are aware of the issues at low Reynolds number where stratification will occur; a dual-path meter configuration would be recommended in such circumstances.

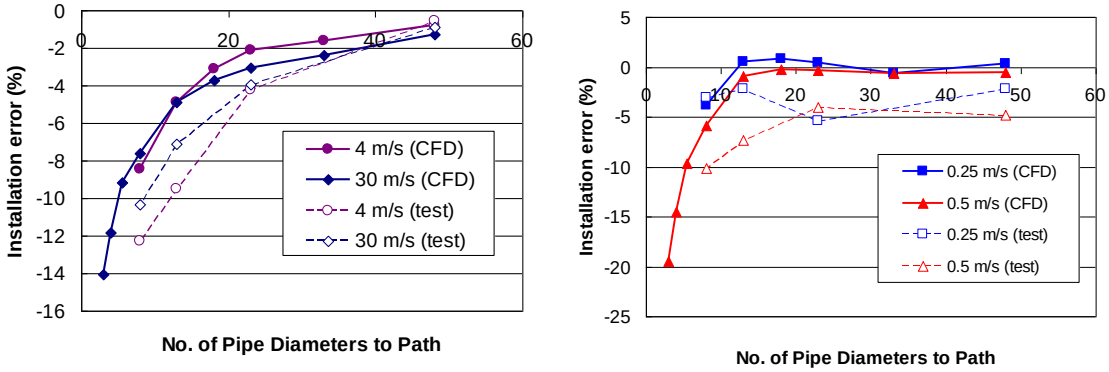

a) b)

Fig. 10 - Comparison of Installation Error Determined by tests and CFD for the diametric Path (Re_D = 80,000 and 600,000)

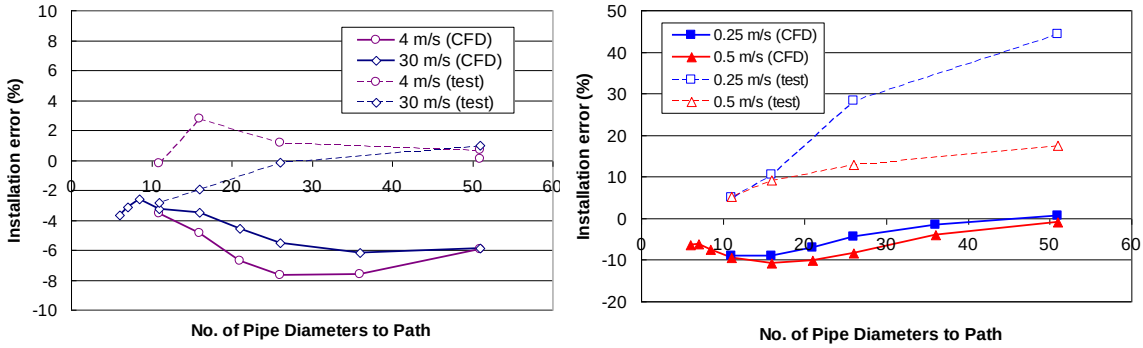

a) b)

Fig. 11 - Comparison of Installation Error Determined by tests and CFD for the mid-radius path
(Re_D = 80,000 and 600,000)

6.1 Comparison of CFD velocity profiles with published LDV data

The question arises as to whether or not the CFD correctly predicts the velocity profiles through the single bend and in the downstream pipe. In order to address this issue, it was decided to compare the predicted velocity profiles with available velocity profiles measured by Laser Doppler Velocimetry (LDV). These data were kindly supplied to TUV NEL by the

National Institute of Standards and Technology (NIST) [10]. The profiles were taken across the horizontal and vertical axes downstream of a single bend tested in water at Re_D = 10,000 and 100,000 and at about 3, 6, 11, 15, 19, 23D from the outlet of a 2-inch single bend.

Figure 12 compares the horizontal and vertical velocity profiles at 3D and 23D downstream of the single bend at Re_D = 10,000 (the results at Re_D = 100,000 were similar). The CFD is in moderately good agreement with the LDV data close to the bend (especially on the horizontal axis), but deviates further downstream, there being more asymmetry in the CFD profiles compared with the LDV data.

Additional CFD modelling revealed that it would require a total of about 75D downstream of the bend before the predicted flow profile recovered back to fully developed.

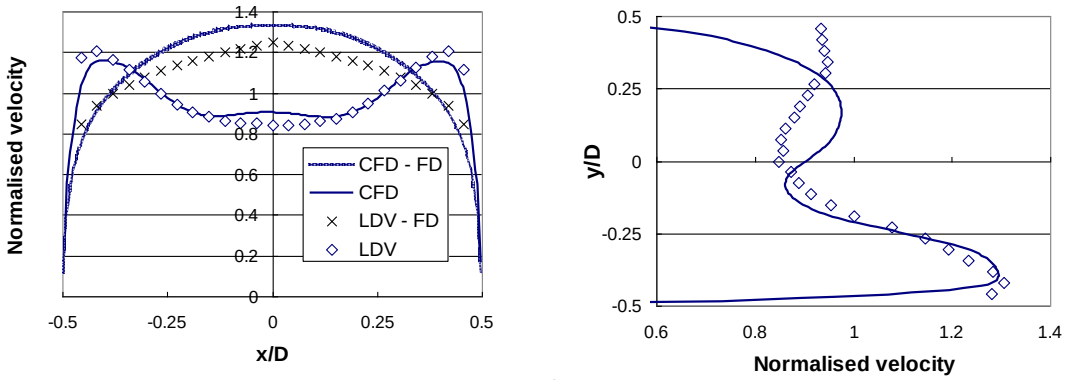

a)

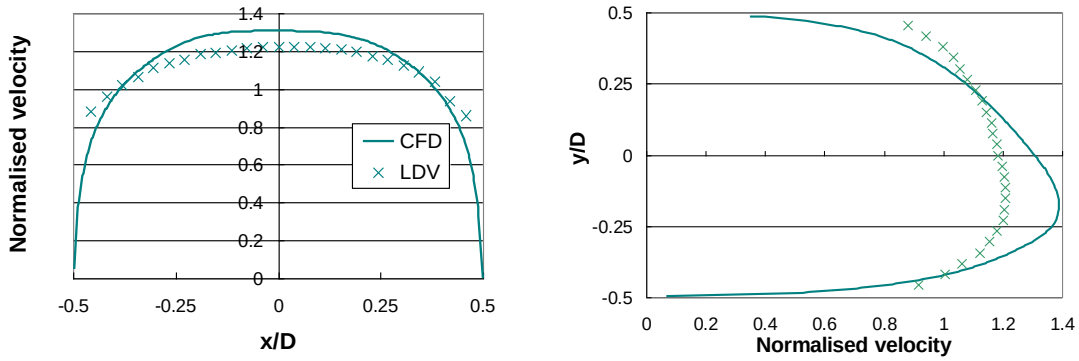

b)

Fig. 12 - Predicted axial velocity on the horizontal (x) and vertical (y) axes compared with LDV data [10]: a) 3D and b) 23D from the bend outlet (Re_D = 10,000)

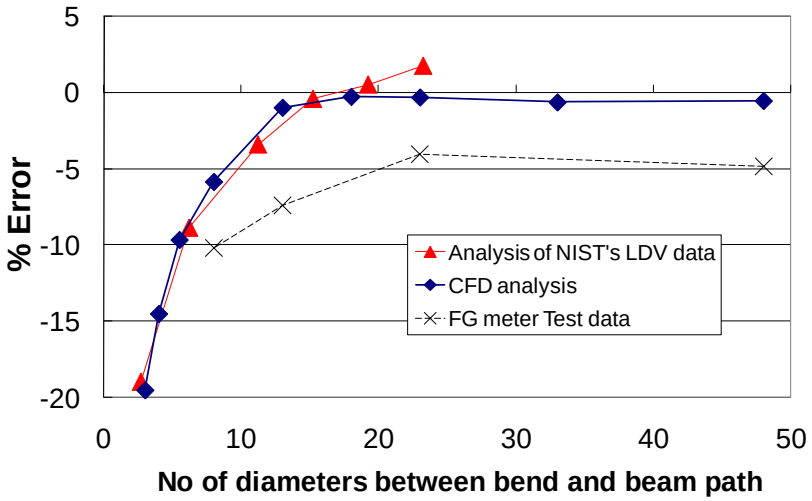

Figure 13 – Comparison of installation error determined from LDV data and CFD analyses with test meter data (Re_D = 10,000)

However, in comparing the fully developed profiles (plotted in Fig. 12a) it is noted that the CFD profile is slightly rounder than the LDV profile. Therefore it might be expected that the velocity profiles downstream of the bend would also differ. It is therefore more appropriate to calculate the percentage shift between the average velocity determined for the disturbed flow case with that of the baseline case. This then gives an approximation to the installation error which can then be compared with the CFD and test data results.

Figure 13 compares the results of analysis of the LDV data with the CFD and meter test data for a velocity of 0.5 m/s (Re_D = 10,000).

The LDV data set was generated by taking the average velocity along the horizontal diameter in fully developed and disturbed flow conditions and calculating the percentage difference between them. It was only possible to do this for the diametric path position.

There is excellent agreement between the CFD and LDV data, which is an encouraging result as it validates the CFD to some degree. However, although the trends in the ultrasonic flowmeter test data are similar, they show a slightly larger shift than the CFD and LDV results perhaps indicating that the flow profiles were not quite the same in the tests on the ultrasonic meter as in the case of the CFD or the LDV data.

6.2 Discussion of CFD results

A single bend generates an asymmetric flow profile that also has non-axial velocity components present. Figure 14 details the velocity contours for the cases of fully developed flow entering the meter (Fig. 14a) and with the meter immediately downstream of the bend (Fig. 14b). The curvature of the bend causes the flow to be thrown to the outside of the pipe creating a skewed velocity profile which will then slowly develop down the pipe. The asymmetry is accompanied by non-axial velocity components (i.e. swirl).

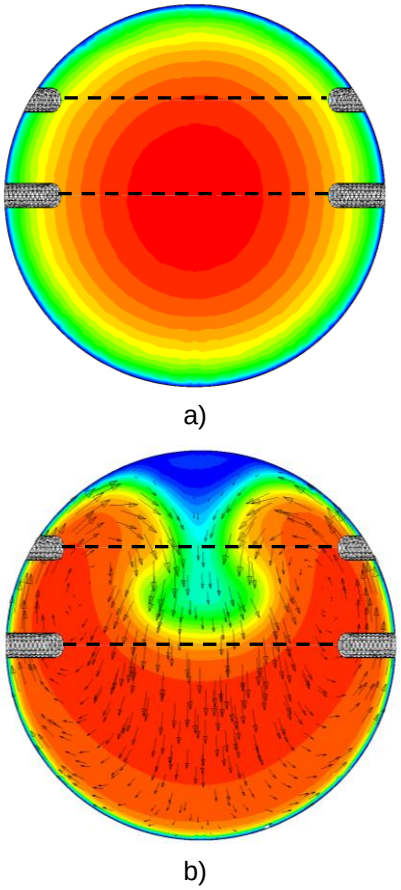

a)

b)

Fig. 14 – Predicted velocity distribution at the meter inlet: a) fully developed flow, b) bend immediately upstream of meter

6.2.1 Effect of swirl

A single bend tends to generate a double, counter-rotating vortex pattern (as shown by the vectors superimposed on Fig. 14b), whilst an out-of-plane double bend tends to generate a single vortex†. In theory, provided the swirl patterns are centred on the axis of the pipe, the diametric path should be less sensitive to swirl than the mid-radius path. This demonstrates the importance of using the method described in Section 5.1 to model installation effect which takes into account both asymmetry and swirl.

6.2.2 Effect of the transducer tips

It was of interest to assess the effect of ignoring the transducer tips in the models. Figure 15 shows how the velocity contours are locally disturbed by the presence of the transducer tips within the CFD model.

Figure 16 details the effect on the installation error if the transducers are not included in the model. The percentage difference between the installation error determined using models without transducers and those with transducers included is plotted against normalised distance from the bend (i.e. number of diameters from the bend to the meter inlet). Apart from the mid-radius beam at 30 m/s, the effect is generally limited to 1%, but it does appear that the intruding transducer tips influence the error more as the bend gets closer to the meter.

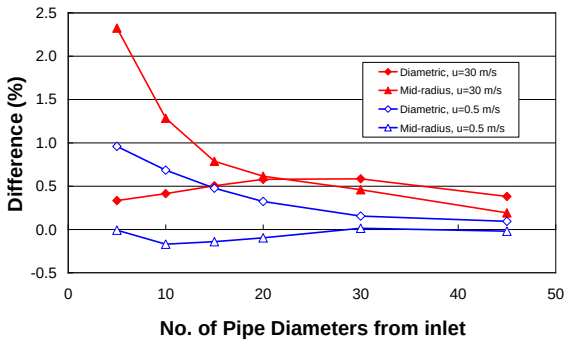

Fig 16 - Effect of modelling the installation error without transducers at 0.5 m/s and 30 m/s

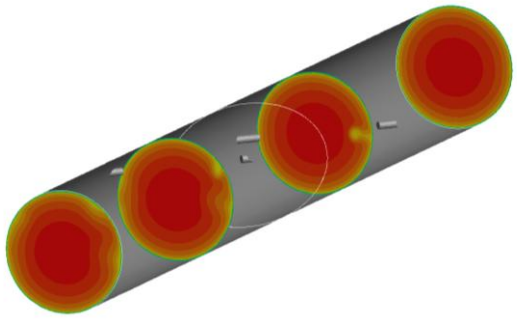

Fig. 15 - Velocity contours through meter model at 30 m/s (fully developed flow at inlet)

† Note: in reality the flow pattern will probably contain elements of both patterns depending on bend separation, Reynolds number, upstream fittings etc.

7 CONCLUSIONS

The CFD simulations agreed well with the test data for the diametric path position and predicted the correct trend with distance from the bend. The predictions were within 2 - 6% of the measurements in all cases. Further confidence is given by the fact that there was excellent agreement between the CFD and published LDV data based on analysis of the velocity profiles along the horizontal diameter.

However the errors at the mid-radius position were significantly different to the test data, especially at the lowest velocities where very large errors were recorded during the tests (i.e. between 5% and about 44%). The error was also seen to increase with distance from the bend, which was somewhat unexpected and counter-intuitive.

There was significantly more scatter on the output from the mid-radius path than on the diametric which may be attributed, in some part, to a disturbance created by the diametric transducers which were only 3 pipe diameters upstream of the mid-radius path. It is also possible that the flow profile was unstable at the lowest velocity tested owing to the flow undergoing laminar-to-turbulent transition. The problems seen at the lowest flow rates are a reflection of the difficulties faced in measuring such low Reynolds number flows – especially considering application to offshore flares where the flare line can be subject to pulsations from winds, temperature differentials etc.

Further technical discussions with GE Sensing have raised the possibility that the signal noise on the mid-radius channel (seen even at zero flow) could have been the result of reflections of the ultrasonic beam occurring due to the transducer tip being so close to the pipe wall. It is possible that the electronic noise could have caused the large variation in meter error at low flow.

The influence of the transducer tips on the resulting installation error was also examined using the CFD. The results were more sensitive to the inclusion of the transducer tips as the bend was moved closer to the meter. This is perhaps as would be expected since the swirl is more intense closer to the bend outlet creating increased interaction of the flow with the transducer tips. There was no obvious trend with velocity.

8 FURTHER WORK

The issues raised in this paper are being examined under an ongoing follow-up project. Some of these are listed below:

- Further testing will be carried out with a modified meter arrangement (i.e. removing the diametric path to observe if there is any effect on mid-radius path). This phase will involve close working with GE Sensing to ensure there are no issues with signal noise etc. resulting from set-up.
- GE Sensing will be supplying a GC868 meter with an additional digital signal processing board that allows a much faster response time (~5 Hz as compared with 0.2 Hz when using the GF868 logging from two channels).
- Inclusion of the transducer bosses in the CFD models.
- CFD modelling of meters with dual- or multi-path transducers to examine the effect on the installation error.

9 ACKNOWLEDGEMENTS

The author wishes to thank Cliff Probert of TUV NEL for carrying out the testing, GE Sensing for the supply of the GF868 flare gas meter and Jed Matson, Hilko den Hollander, Gordon Mackie and colleagues at GE Sensing for their advice and technical support during this project.

10 NOTATION

D	Pipe diameter
k	Meter factor
L	Path length
Q	Volumetric flowrate
R	Pipe radius
t_{12}	Transit time in upstream direction
t_{21}	Transit time in downstream direction
Δt	Transit time difference
v	Velocity
ϕ	Beam angle

11 REFERENCES

[1] TUV NEL Report 2008/301 Installation effects on a flare gas ultrasonic meter (Draft)

[2] Directive 2003/87/EC of the European Parliament and of the Council of 13 October 2003 establishing a scheme for greenhouse gas emission allowance trading within the Community and amending Council Directive 96/61/EC (http://ec.europa.eu/environment/climat/emission/implementation_en.htm)

[3] Establishing Guidelines for the monitoring and reporting of greenhouse gas emissions pursuant to Directive 2003/87/EC of the European Parliament (2007) (http://eurlex.europa.eu/LexUriServ/site/en/oj/2007/l_229/l_22920070831en00010085.pdf)

[4] BRITISH STANDARDS INSTITUTE. Guide to the selection, installation, operation and calibration of diagonal path transit time ultrasonic flowmeters for industrial gas applications, BS 7965 2008.

[5] INTERNATIONAL STANDARD ORGANISATION. Measurement of fluid flow in closed conduits - methods using transit-time ultrasonic meters, BSI ISO/TR 12765, 1998.

[6] Hydrocarbon Management Committee. Determination of flare quantities from upstream oil and gas facilities, HM58, Energy Institute, London, May 2008.

[7] INTERNATIONAL STANDARD ORGANISATION. Measurement of fluid flow in closed conduits - Part 2: Orifice plates. ISO 5167-2, Geneva: International Organization for Standardisation, 2003.

[8] ANSYS Fluent website http://www.fluent.com/

[9] Versteeg, H.K., and Malalasekera, W. An Introduction to Computational Fluid Dynamics - The Finite Volume Method. Longman Scientific and Technical Publications, New York, 1st Ed., 1995.

[10] T.T. Yeh, National Institute of Standards and Technology, Gaithersburg, MD. Private communication, 2000.